Microstructural evolution in single tungsten fiber-reinforced tungsten composites during annealing: recrystallization and abnormal grain growth

Umberto M. Ciucani[1]*, Lea Haus[1], Hanns Gietl[2,3], Johann Riesch[2], Wolfgang Pantleon[1].

[1] *Section for Materials and Surface Engineering, Department of Mechanical Engineering, Technical University of Denmark, 2800 Kongens Lyngby, Denmark;*

[2] *Max-Planck-Institut für Plasmaphysik, 85748 Garching, Germany.*

[3] *Technische Universität München, 85748 Garching, Germany.*

***Corresponding Author:** Umberto M. Ciucani, Section for Materials and Surface Engineering, Department of Mechanical Engineering, Technical University of Denmark, 2800 Kongens Lyngby, Denmark, umciuc@mek.dtu.dk, +45 45254883.

Corresponding Author ORCID: orcid.org/0000-0003-3881-4811

Microstructural evolution in single tungsten fiber-reinforced tungsten composites during annealing: recrystallization and abnormal grain growth

Tungsten is considered as plasma-facing material in future fusion reactors. Due to the high operation temperatures, the occurrence of microstructural restoration processes as recovery, recrystallization and grain growth will unavoidably alter the desired microstructure obtained after processing and impede otherwise beneficial mechanical properties. Potassium-doping proved to be efficient in hindering or at least delaying such phenomena. Tungsten fiber-reinforced tungsten composites with drawn tungsten wires embedded in a tungsten matrix show a certain pseudo-ductility. Cylindrical single fiber composites with a single potassium-doped drawn tungsten wire in a chemically vapor deposited tungsten matrix, with or without a rare-earth oxide interlayer, were investigated as model systems. Individual specimens were annealed at 1400 °C up to four weeks and changes in their microstructure tracked by electron backscatter diffraction. In the as-processed condition, the tungsten matrix showed large wedge-shaped grains stretching radially from either the interface between matrix and wire or the oxide interlayer to the outer surface with very small grains in the vicinity of the interface/interlayer. Upon heating, two zones with larger grains compared to the as-processed condition developed: in the wire regions close to its perimeter primary recrystallization led to formation of new grains with orientations deviating slightly in alignment of their crystallographic <110> directions with the wire axis compared to the drawn wire. In the matrix, abnormally grown grains consumed the as-deposited microstructure in the vicinity of the interface/interlayer. Without an interlayer, abnormally growing grains from the matrix invaded the recrystallizing wire progressively consuming the wire. Both erbia and yttria interlayers efficiently prevented abnormally growing grains from invading the wire (except at few occasions where the oxide interlayer presented imperfections). In this manner, the presence of an interlayer becomes crucial for retaining an interface essential for the pseudo-ductility of the composite.

Keywords: tungsten fiber-reinforced tungsten; recrystallization; grain growth; microstructural evolution; thermal stability; EBSD.

1. Introduction

Fusion is set to become one of the major means of world energy production in future. The operation of fusion reactors impose demanding working conditions [1] and strong requirements on the materials [2]. Armor material of plasma-facing components will face extreme heat and particles fluxes requiring an outstanding heat resistance in combination with a fast heat transport.

Tungsten (W) and tungsten alloys are considered the main candidate materials for plasma-facing components thanks to superior characteristics of tungsten: low-activation, high thermal conductivity, low sputtering yield, high strength and creep resistance at elevated temperatures [3–6]. Due to its body centered cubic lattice and high melting temperature, pure annealed tungsten has a high brittle-to-ductile transition temperature and behaves brittle at room temperature [4,7–10] restricting its use as plasma-facing material, whereas plastically deformed tungsten in general behaves more ductile at ambient temperatures. Large plastic deformation has been utilized for more than hundred years for fabrication of ductile tungsten wires by wire drawing [11]. Efforts are currently undertaken to lower the brittle-to-ductile transition temperature of tungsten plates even below room temperature also by cold rolling [12].

Unfortunately, the deformation structures obtained by plastic deformation are not stable at the operation temperatures of 800 °C and above of plasma-facing components. During operation, they will undergo restoration processes altering the microstructure by recovery, recrystallization and grain growth [13,14]. In particular, recrystallization consisting of nucleation and growth of defect-free grains at the expense of the ductile matrix will reinstate the intrinsic brittleness of tungsten.

Several pure tungsten plates warm- or cold-rolled to different rolling reductions have been studied in terms of their thermal stability (see e.g. [15–21]). Moderately rolled tungsten plates (see [15–19]) are sufficiently thermally stable to withstand microstructural changes at the expected temperatures of 800 °C for the first wall, but will not be able to endure the higher expected divertor temperatures of 1100 °C and above for the required two years.

Attempts to improve the mechanical properties of tungsten focus on ductilization by means of alloying (Re, Ti, Ta and V, e.g. [22,23]) or dispersion strengthening by oxides or other particles (Y_2O_3, La_2O_3 or TiC, see e.g. [24,25]). Particle dispersions provide an additional advantage as they stabilize deformation structures by preventing boundary migration through Zener pining [26].

Similar to impeding boundary motion by particle dispersions, doping with potassium has been utilized for preventing tungsten wires from losing their beneficial mechanical properties obtained after wire drawing through undesired microstructural restoration processes [11]: During processing, insoluble potassium forms potassium bubbles which impede grain boundary motion and stabilize the microstructure of the drawn wires. In this manner, ductile wires with sufficient life time at high temperature are achieved and successfully applied in commercial light bulbs. More recently, attempts were undertaken to utilize potassium-doping also for cold-rolled tungsten plates (e.g. [21]).

As an alternative to bulk tungsten material, pseudo-ductile tungsten fiber composites are considered where tungsten (W) is chemically vapor deposited as matrix material on drawn potassium-doped tungsten wires forming reinforcing fibers (W_f) [27,28]. Such tungsten fiber-reinforced tungsten (W_f/W) composites consist of two different "phases" with rather different properties, both formed by almost pure tungsten: the chemically vapor deposited tungsten matrix behaves brittle, whereas the drawn tungsten wires are able to deform plastically under mechanical load. The plastic work required for their deformation as well as the energy dissipation at the interface between wire and matrix will prevent crack propagation and ensure a certain pseudo-ductility of the composite [29,30]. Multifilament composites with tungsten deposited on layered meshes of drawn tungsten wires are considered for plasma-facing components [31,32]. The debonding behavior between fibers and matrix during mechanical loading of multifilament composites with parallel fibers has been investigated in the as-processed state as well as in an embrittled state after annealing for 30 min at 1727 °C [30,31].

A model system containing a single tungsten fiber in a tungsten matrix can elucidate the crucial role of the interface between wire and matrix for the behavior of the composite. Different interlayers have been applied to modify the cohesive properties and to improve the mechanical behavior [27,33]. Until now, the microstructure of single fiber composites has been investigated with respect to cohesion and integrity of the interlayer only during short time annealing at a temperature of 800 °C [33].

In view of the importance of thermally stable microstructures for the performance of W_f/W composites under operation conditions in a fusion reactor, the microstructural evolution in single fiber composites with and without a rare-earth oxide interlayer is investigated here during isothermal annealing at 1400 °C for long terms up to 28 days. Future investigations at lower temperatures will establish the temperature dependence of the observed phenomena allowing extrapolation of the findings to the operation temperature of plasma-facing components.

2. Materials and Methods

Single fiber composites containing a single tungsten wire in a chemically vapor deposited tungsten matrix are investigated as models system for tungsten fiber-reinforced tungsten composites (W_f/W). The geometry of such cylindrical single fiber composites is illustrated in Fig. 1, their production detailed in [29,30,33]. Tungsten wire doped with 60 ppm potassium and drawn to a diameter of 150 µm were provided by OSRAM GmbH. Pure tungsten is deposited by chemical vapor deposition (CVD) directly on the wire at temperatures between 580 °C and 620 °C through the chemical reaction

$$WF_6 + 3\,H_2 \rightarrow W + 6\,HF \qquad (1)$$

In this manner, cylindrical specimens with larger diameter of 3.0±0.1 mm are achieved. Additional to single fiber composites without any interlayer, two different single fiber composites with a thin rare-earth oxide interlayer are produced. For this, the drawn tungsten wires were coated

in a two-step process by reactive magnetron sputtering with a 1 µm thin layer of either erbia (Er_2O_3) or yttria (Y_2O_3), before the tungsten matrix is grown by CVD. Cylindrical single fiber composite specimens with diameters of 1.5±0.1 mm and 2.1±0.1 mm are obtained for erbia and yttria coated tungsten wires, respectively.

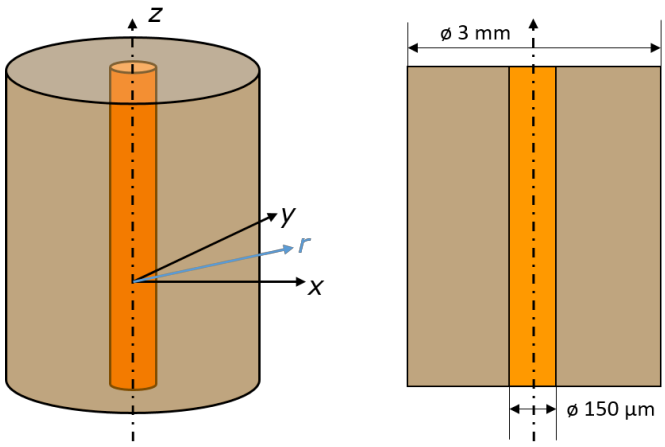

Figure 1. Sketch of the geometry of single fiber W_f/W composites (not to scale). Upon a drawn potassium-doped tungsten wire with a diameter of 150 µm (dark orange), tungsten is chemically vapor deposited (shown in light orange) - either without interlayer (as sketched) or with an oxide interlayer physically vapor deposited on the wire before CVD of the matrix (not shown). The radial direction *r* in a transversal (*xy*) plane perpendicular to the wire axes (i.e. in a cross section) points outwards from the wire center as indicated.

From the produced cylindrical single fiber composites, disc-shaped samples were cut to a height of 1.35±0.05 mm. In order to remove the mechanically induced deformation layer, one of the cut surfaces was mechanically grinded (with SiC-paper of subsequent grit sizes 800, 1200, 2500 and 4000) and chemo-mechanically polished (with different oxide particle suspensions) and only this surface was investigated further. For protection of the specimens against oxidation and formation of volatile WO_3 during annealing treatments, specimens were encapsulated in quartz glass ampoules (either individually or together with other specimens having different interlayers). The procedure consists of evacuating the ampoules, flushing them with Argon (with purity higher than 99.999%), and finally sealing them with a blowtorch. Isothermal annealing of encapsulated specimens at

1400 °C was performed for up to 28 days (672 h). The ampoules were put in a pre-heated ceramic tube furnace NaberTherm RHTC 80-230/15, removed after the desired annealing time and cooled to room temperature by air-cooling. For four different annealing times (7 days, 14 days, 21 days and 28 days), the microstructure of a single specimen was investigated for each of the three different types of single fiber W_f/W composites.

For microstructural investigations, one of the two surfaces of the specimens (corresponding to cross sections of the single fiber composites) were prepared using a standard metallographic route consisting of mechanical grinding (on SiC-paper of grit size 2000 and 4000), polishing (with diamond suspension with grain size 3 µm), and final electro-polishing using an aqueous solution containing 3 wt.% NaOH at room temperature with an applied voltage of 12 V and a current of approximately 2 A.

EBSD investigations on freshly prepared samples were accomplished using a Bruker NOVA NanoSEM equipped with a Bruker e-Flash HD EBSD detector applying a voltage of 20 kV to investigate either the entire cross sections or specifically the regions around the original wire and the wire itself. Maps were obtained with different magnifications and different step sizes Δx: Large overview maps of the entire cross section were recorded at lowest magnification with a step size of 5 µm. For revealing the microstructural details of the tungsten wire and the region just around it, a higher magnification and smaller step sizes of 150 nm and 500 nm were used for the as-processed state and the annealed conditions, respectively. The reason for recording maps with different step sizes is routed in the necessary compromise between sufficient resolution for the analysis of the microstructural details in the wire and a reasonably short acquisition time for the entire CVD region. Without any filtering or removal of non-indexed points, the gathered EBSD data are analyzed using the MTEX toolbox [34] and evaluated further by own purposely developed routines.

3. Results

3.1. As-processed condition

The microstructure of the single fiber W_f/W composites in their as-processed condition is presented in Fig. 2 where secondary electron images of cross sections of a specimen without any interlayer (Fig. 2(a-b)) and a specimen with an erbia interlayer (Fig. 2c) are shown. In both cases, the drawn wire and the CVD matrix can be clearly distinguished. Due to the drawing process, tungsten grains in the wire are fibrous and elongated along the wire drawing direction (e.g. [35]). Their extremely small cross sections cannot be resolved individually even with the higher magnification of Figs. 2(b-c). On the other hand, large tungsten grains can be observed in the CVD matrix in Fig. 2a. These grains are elongated radially, i.e. along their growth direction during the deposition process. Their azimuthal width (i.e. their width along a circle of constant radius) increases with increasing distance from the center. Some of the wedge-shaped grains even grow radially through the entire deposited layer from the vicinity of the wire all the way to the outer surface (cf. Fig. 2a). The geometry of these wedge-shaped grains will be explored further based on EBSD data. In matrix regions in the vicinity of the wire, very small grains are observed which are slightly elongated, but not as much as the wedge-shaped grains in the outer region. The location of the oxide interlayer can also be clearly identified from the groove caused by electro-polishing for the specimen with an erbia interlayer in Fig. 2c. From the appearance of the oxide interlayer in Fig. 2c as well as from the discernable interface between matrix and wire in Fig. 2b of the specimen without an interlayer, it becomes obvious that the wire does not exhibit a perfect circular cross section. Several extrusion and intrusion can be clearly recognized.

(a)

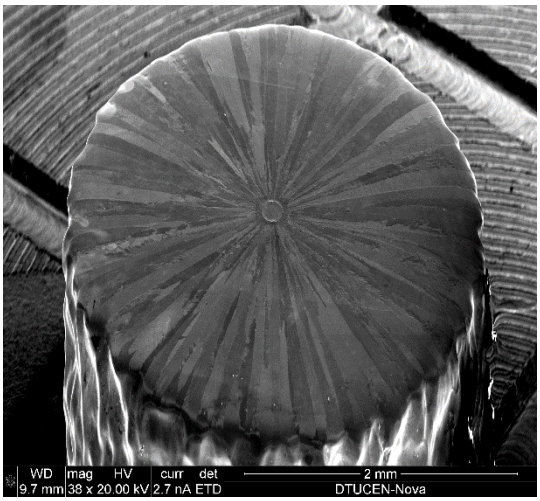

(b)

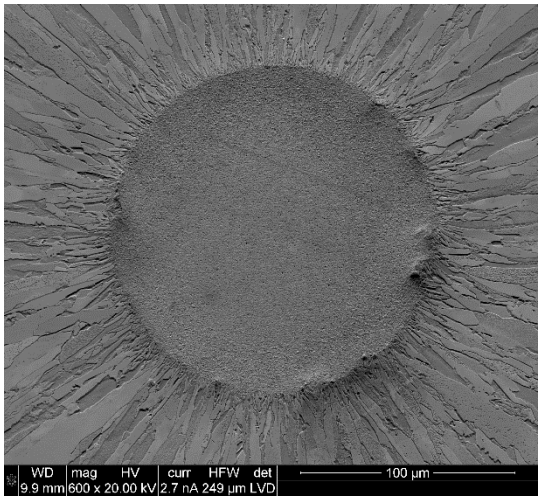

(c)

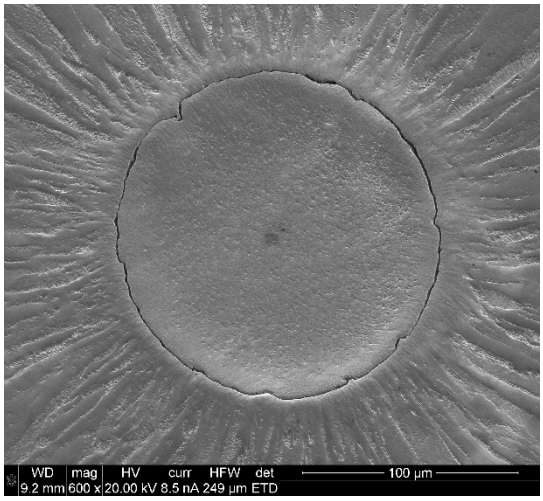

Figure 2: Secondary electron images obtained by scanning electron microscopy on cross sections of single fiber W_f/W composites in their as-processed condition: composite without interlayer (a) with smallest possible magnification and (b) with highest recorded magnification; (c) composite containing an erbia interlayer (obvious from the groove caused by electro-polishing) at highest recorded magnification.

A more detailed assessment of the as-processed microstructure is enabled by orientation mapping by means of EBSD. Fig. 3 shows orientation maps obtained on all three different types of single fiber W_f/W composite. Grains in the matrix are easily discerned. Obviously, these grains are elongated along the radial direction, i.e. the direction pointing outwards from the wire center in the cross sectional view. Their increasing width with distance from the center confirms the observation of wedge-shape grains in Fig. 2a.

All overview maps (Figs. 3 a-c) reveal that with the small magnification chosen it becomes impossible to determine the orientation of tungsten grains in the wire. Almost none of the points in the wire could be properly indexed. This is different for the detailed maps obtained with higher magnification where a high indexing rate is achieved also for points in the wire. Most of the points in the wire appear green, revealing the preference for a crystallographic <110> direction along the wire axis as expected for a body centered cubic metal after wire drawing [36,37]. In the center maps of the specimens with an oxide interface (Fig. 3(e.f)), the position of the interlayer is clearly delineated by the presence of non-indexed points. (For determination of the phases and orientations present in the oxide layers, the conditions for recording ESBD patterns would have to be improved even further.) Contrarily, in the CVD matrix, different grains can be clearly distinguished from their different color (mainly red, yellow and green) revealing different crystallographic directions (from <100> to <110>, correspondingly) along the wire axis.

In order to reveal microstructural details quantitatively, disorientations between neighboring points are determined from the orientations gathered by EBSD and boundaries identified in the maps (Figs. 3(a-c) and (g-i)). For each indexed point, the upper and the left neighbors are considered, if they are indexed points as well. If the disorientation angle is above 2° the presence of a boundary is presumed. High angle boundaries (HABs) with disorientation angles above 15° are distinguished from low angle boundaries (LABs) with disorientation angles between 2° and 15°. Most of the identified boundaries in the outer regions of the matrix are aligned along the radial direction delineating clearly the wedge-shaped grains. Several of the grains, show a continuous increase in width with increasing distance from the center and the boundary density decreases in the outer regions. Some of them have grown apparently through the entire deposition process of the CVD matrix. In the matrix regions in the vicinity of the wire, many smaller, not as elongated grains are observed and a radial alignment of the boundaries is not pronounced.

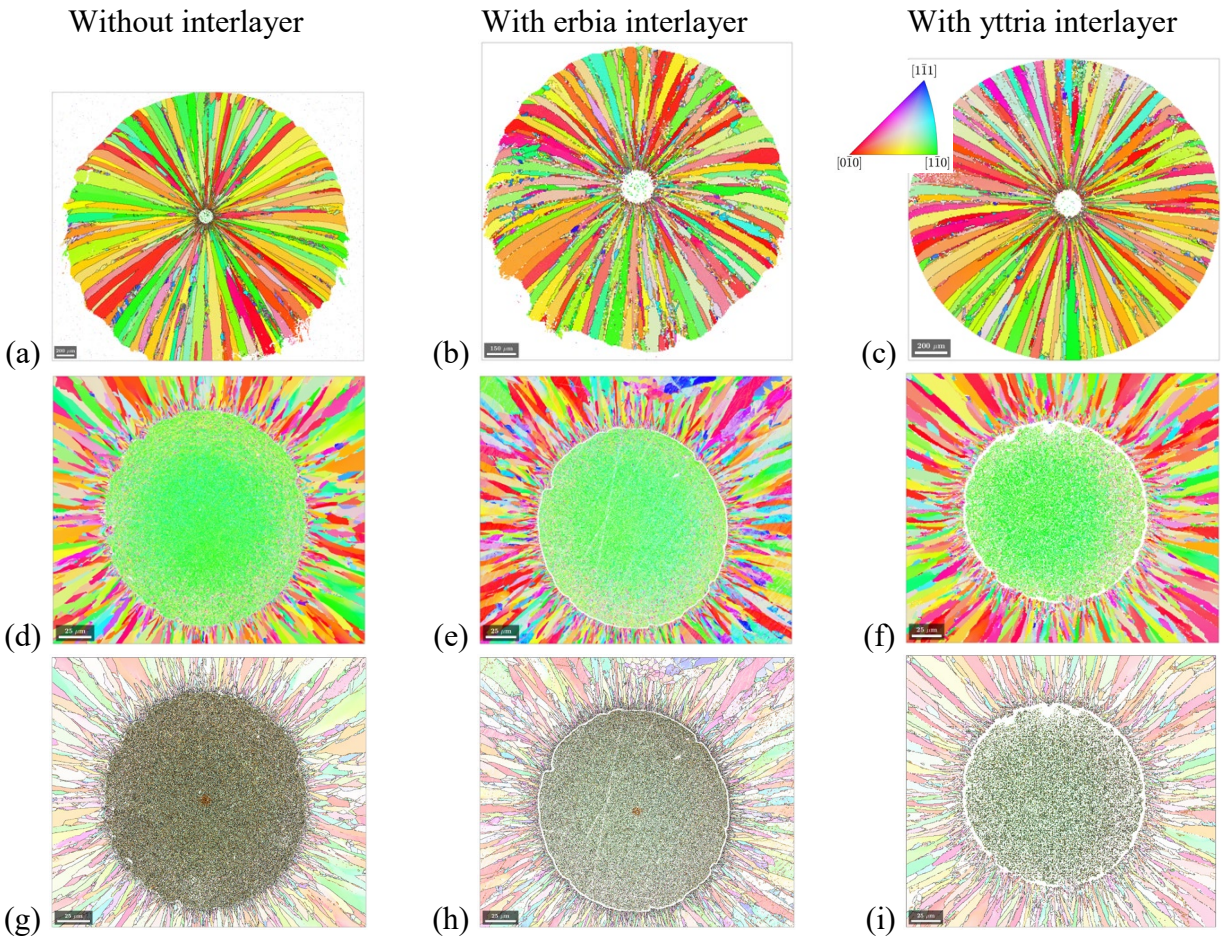

Figure 3: Orientation maps obtained by EBSD on cross sections of single tungsten fiber-reinforced tungsten composites W_f/W with and without an oxide interlayer: left column (a,d,g) without any interlayer, center column (b,e,h) with erbia interlayer and right column (c,f,i) with yttria interlayer. (a-c) present large overview maps all obtained with a step size of 5 µm (but shown with different magnification), (d-i) smaller maps of the wire and its vicinity with a step size of 150 nm. The coloring reflects the crystallographic direction along the wire axis, corresponding to the inset in (c). Boundaries are highlighted in (a-c) and (g-i): High angle boundaries with disorientation angles above 15° in black and low angle boundaries with disorientation angles between 2° and 15° in light brown. In the boundary maps (g-i) the colors representing orientations are rendered transparent.

For characterizing the microstructure in dependence on the radial distance r from the wire center, all indexed points of a map in a ring with radius r and a width corresponding to the step size Δx are considered. Their number in an interval between r and $r + \Delta x$ are counted (N_{points}) as well as the number of high angle boundaries to their left (N_{left}) and upwards (N_{up}). The mean spacing between

high angle boundaries along such a ring follows, consequently, as ratio between the perimeter length of the ring formed by indexed points (given by $N_{\text{points}}\Delta x$) and the total number of high angle boundaries

$$\lambda = \frac{N_{\text{points}}\Delta x}{N_{\text{left}} + N_{\text{up}}} \tag{2}$$

The relevance of the proposed evaluation procedure is illustrated for the as-processed condition of the tungsten fiber-reinforced tungsten composite with an erbia interlayer. For the large orientation map presented in Fig. 3b, quantitative analysis of the boundary spacing is only possible in the CVD matrix (i.e. for radii between 75 µm and 750 µm as seen in Fig. 4a) as points in the wire could not be indexed when acquiring the data with a large step size Δx of 5 µm and small magnification. On the other hand, when acquiring data with a finer step size Δx of 150 nm, the patterns could be more reliably indexed (in Fig. 3h) and orientation information in the wire, i.e. for radii below 75 µm, becomes available (cf. Fig. 4b).

Fig. 4a reveals that the HAB spacing in the CVD matrix depends almost linearly on the radius r, at least up to radii of 450 µm. In this region, the slope $\varphi = d\lambda/dr = 0.042 = 2.4°$ of the curve in Fig. 4a is rather constant showing (i) that the number of HABs along a perimeter given by $2\pi/\varphi \approx 150$ is constant (confirming the earlier visual impression from the orientation maps) and (ii) that the number of grains does not increase with increasing radius. Instead, all grains grow out radially and develop a wedge shape covering in average an angle φ of 2.4° as reflected in the orientation map in Fig. 3b.

As obvious from Fig. 4a, the linear increase of the HAB spacing does not continue for radii above 450 µm. In this outer region, the emergence of additional grains can be identified by careful inspection of the orientation map in Fig. 3b. (Along the perimeter of a ring with radius 600 µm, for instance, about 200 high angle boundaries can be identified, i.e. substantially more than the constant number of 150 reported above along perimeters for radii below 450 µm.) The reason for the

occurrence of further grains and the impeded azimuthal growth of the wedge-shaped grains might be either lateral growth of neighboring grains along the wire direction or local disturbances in the deposition process causing the formation of grains with new orientations.

As seen from Fig. 4b obtained from the more detailed orientation map of the center region (Fig. 3h), the linear dependence of the HAB spacing on the radius in the CVD matrix continues undisturbed to lower radii almost entirely towards the erbia interlayer. In the wire itself, the spacing between high angle boundaries with 0.42 µm is almost constant with possibly a slight decrease towards the wire edge. This is considered as an effect of heterogeneous deformation during wire drawing (from contact with the die) and not observed in all as-processed specimen. As noted earlier, the erbia interlayer is not exactly located at 75 µm around the entire perimeter, some intrusion and extrusions are seen. Due to these local deviations from cylindrical symmetry, information on the spacing between HABs gets averaged between matrix and wire in regions close to the interlayer.

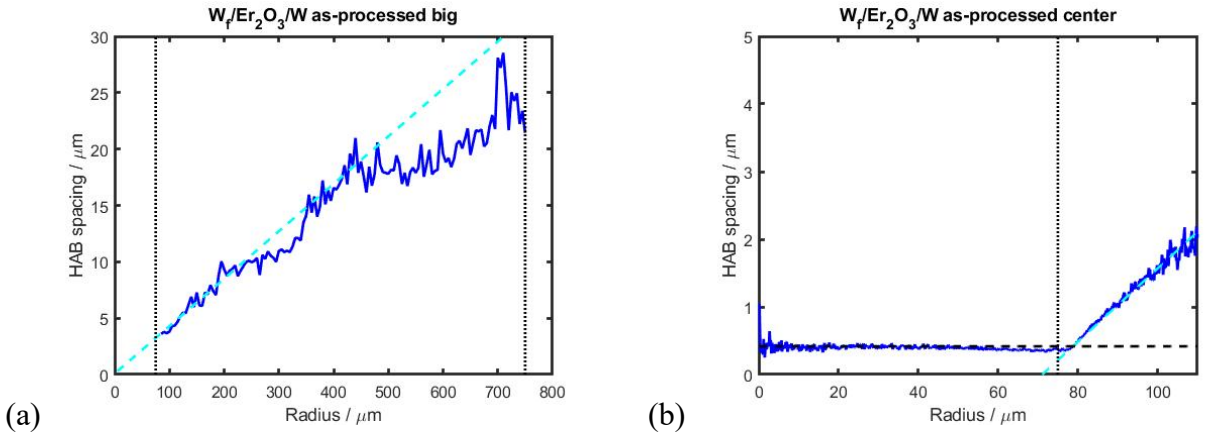

(a) (b)

Figure 4: High angle boundary spacing λ (according to eq. (2)) in dependence on the distance from the center of the wire for a tungsten fiber-reinforced tungsten composite with an erbia interlayer in the as-processed condition as obtained (a) from the overview map in Fig. 3b and (b) from the center map in Fig. 3h. The dotted, black lines represent the positions of the interlayer at a radius of 75 µm and the outer surface. The dashed, cyan lines are fits of a linear dependence of the HAB spacing on the radius in the CVD matrix. The dashed, black line in (b) illustrates the constant HAB spacing in the center of the wire.

3.2. Annealed condition

Orientation maps from single fiber composites with an erbia interlayer after annealing for four different times up to 28 days are presented in Fig. 5. Marked differences to the as-processed condition in Fig. 3e and 3h are observed: larger grains (compared to the as-processed condition) can be identified in the orientation map after annealing on both sides of the interlayer. In particular, the very small, slightly elongated grains just outside the interlayer are replaced by larger grains which differ strongly in their morphology from both the grains they replaced and the grains further out. They are almost equiaxed and extend only slightly more along the radial direction than along the azimuthal direction. Obviously, they do neither reach the aspect ratios observed before annealing in that region close to the interlayer, nor the extreme ratios of the wedge-shaped grains still remaining in the outer regions.

Within the wire, small grains of slightly deviating orientation can be recognized by their yellow or lilac colors contrasting the dominant green color in the as-processed condition, indicating that the alignment of the crystallographic <110> direction with the wire axis is not as pronounced as before annealing. These newly emerging grains in the outer region of the wire are larger than the original fibrous grains in the as-processed condition as they are clearly revealed from the orientation map, despite its larger step size of 500 nm compared to the one (150 nm) of Fig. 2c. These emerging grains are considered to be free of defects and do not contain any deformation structures as neither LABs, nor color differences indicating disorientations within them are discerned.

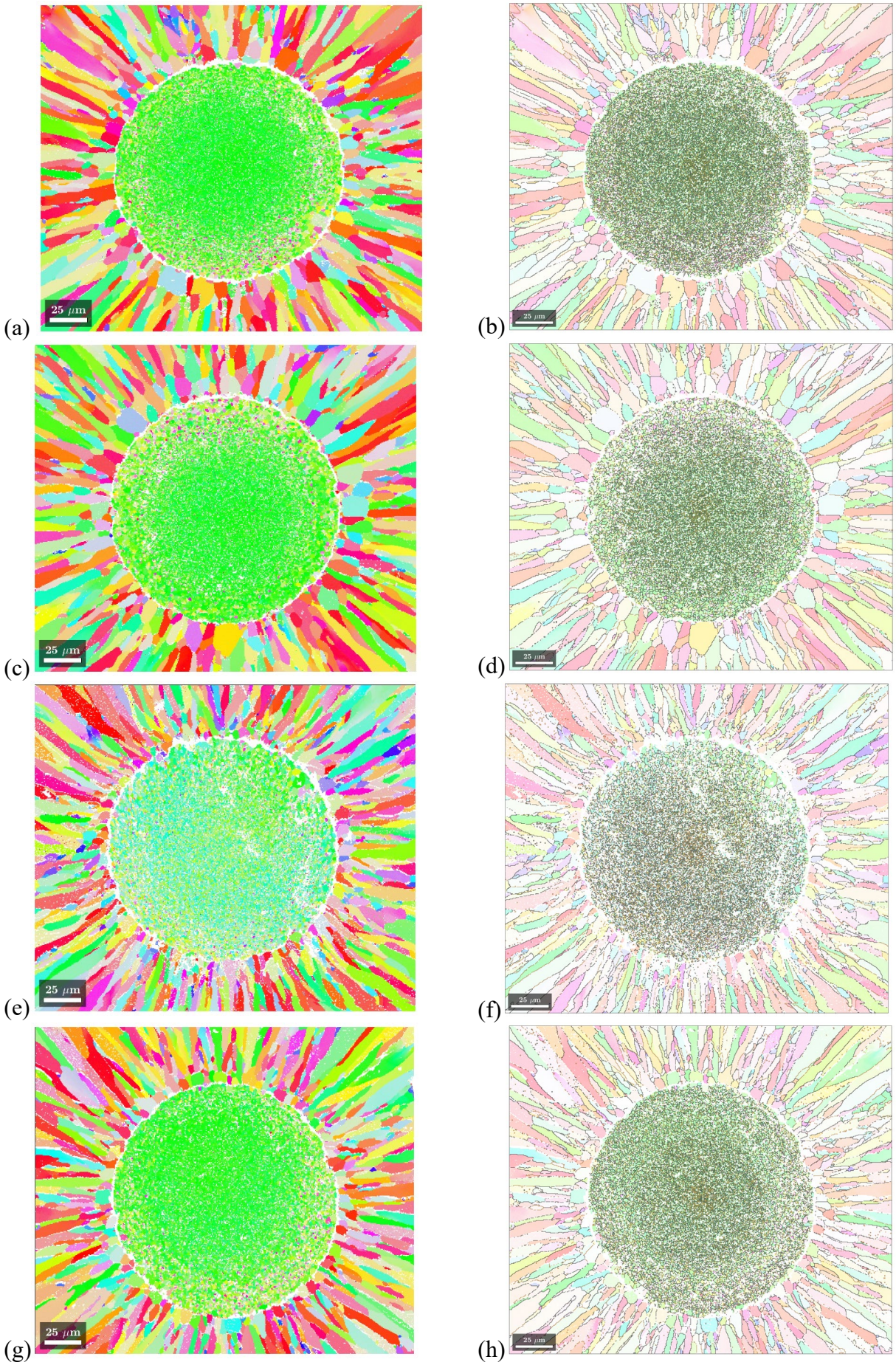
(a)
25 μm
(b)
25 μm
(c)
25 μm
(d)
25 μm
(e)
25 μm
(f)
25 μm
(g)
25 μm
(h)
25 μm

Figure 5: Orientation maps of the wire and its vicinity obtained by EBSD with a step size of 500 nm on cross sections of single tungsten fiber-reinforced tungsten composites with an erbia interlayer after annealing at 1400 °C for different times: (a,b) 7 days, (c,d) 14 days, (e,f) 21 days and (g,h) 28 days. The coloring reflects the crystallographic direction along the wire axis, corresponding to the inset in (b). Boundaries are highlighted in the right column (b,d,f,h): High angle boundaries with disorientation angles above 15° in black and low angle boundaries with disorientation angles between 2° and 15° in light brown. In the boundary maps (b,d,f,h) the colors representing orientations are rendered transparent.

These observations are further substantiated by determining the spacing between HABs in different distances from the wire center as shown for the single tungsten fiber-reinforced tungsten composites W_f/W with an erbia interlayer after annealing at 1400 °C for 28 days in Fig. 6.

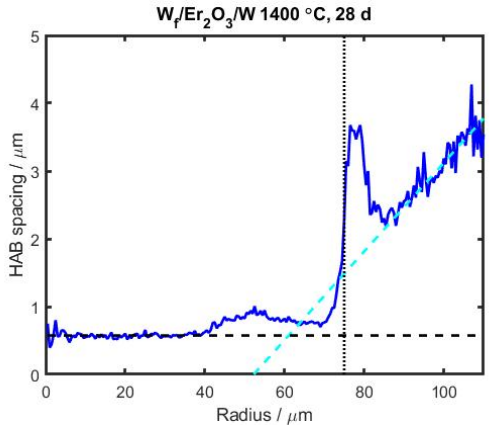

Figure 6: High angle boundary spacing λ (according to eq. (2)) in dependence on the distance from the center of the wire for a tungsten fiber-reinforced tungsten composite with an erbia interlayer after annealing at 1400 °C for 28 days as obtained from the center map in Fig. 5h. The dashed, cyan line is a fit of a linear dependence of the HAB spacing on the radius in the outer regions of the CVD matrix. The dashed, black line illustrates the constant HAB spacing in the center of the wire. The dotted, black line represents the position of the interlayer at a radius of 75 µm.

From Fig. 6, the occurrence of a zone with large grains can be identified in the CVD matrix in the vicinity of the interlayer with grains much larger than in the as-processed condition, but still small compared to the wedge-shaped grains. From the HAB spacing profile obtained after annealing for 28 d at 1400 °C, a 10 µm wide large grain zone from the interlayer (at 75 µm) to a radius of about 85 µm becomes obvious. Within this zone, the HAB spacing increased from about 0.5 µm close to the interlayer in the as-processed condition to nearly 4 µm revealing the presence of much larger grains and a significant decrease in boundary density.

The observation of a second zone of larger grains within the wire is clearly supported by Fig. 6. For radii between 40 µm and 75 µm, an increased boundary spacing up to 1 µm is detected which is significantly larger than both, the one in the center of the wire (0.57 µm) and the one in the as-processed condition (0.42 µm). The slightly higher HAB spacing of 0.57 µm in the center of the wire (up to radii of 30 µm) compared to the as-processed condition (0.42 µm) is attributed to the slightly larger step size of 500 nm used which does not allow resolving boundary spacings smaller than 0.5 µm.

As seen in Fig. 5, the development of two zones (one in the matrix, the other in the wire) with larger grains than in the as-processed condition is observed – albeit to a different extent – in all single fiber composites with an erbia interlayer annealed for 7 d, 14 d, 21 d or 28 d.

The orientation maps of all three different types of single fiber composites (without any interlayer, with either an erbia or an yttria interlayer) after annealing at 1400 °C for 28 days in Fig. 7 reveal also two zones of larger grains developing in each composite. The development of these zones seems a universal behavior of all investigated single fiber composites, but the extent of the zones and their specific location depend on annealing time and the presence of an interlayer. While both single fiber composites with an oxide interlayer behave rather similar, the large grain zones appear strikingly different in the single fiber composite without any interlayer. This difference and its consequences will be discussed in more detail in section 4.3.

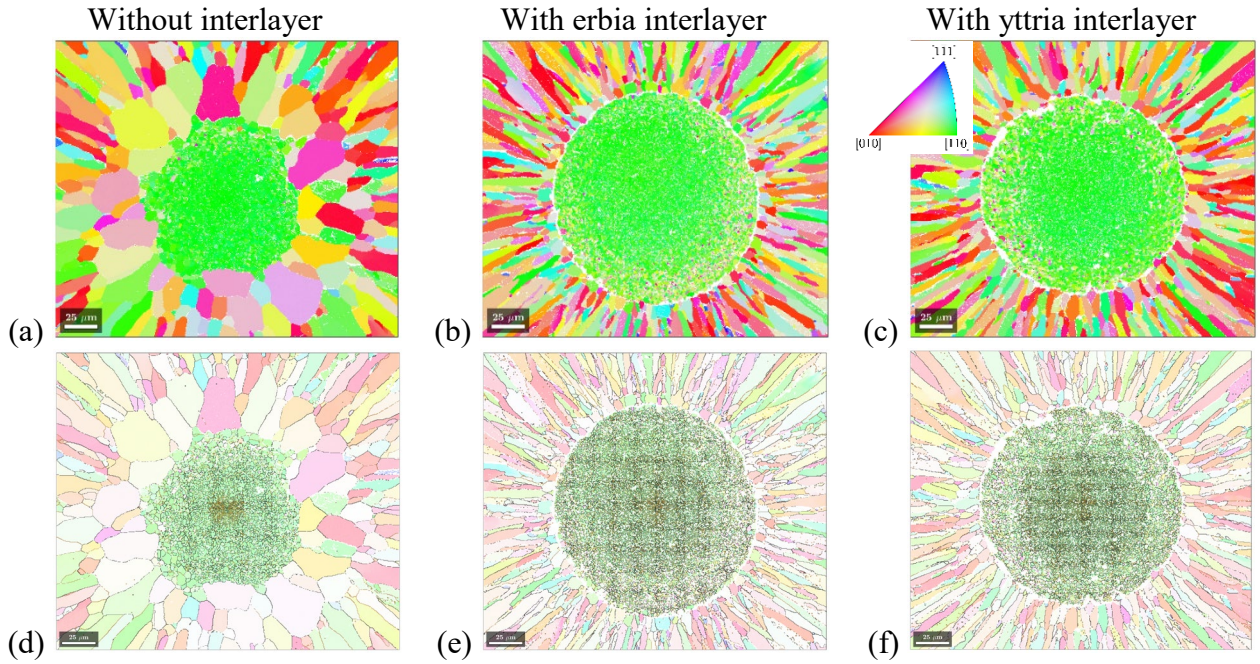

Figure 7: Orientation maps of the wire and its vicinity obtained by EBSD with a step size of 500 nm on cross sections of single tungsten fiber-reinforced tungsten composites W_f/W with and without an oxide interlayer after annealing at 1400 °C for 28 days: left column (a,d) without any interlayer, center column (b,e) with erbia interlayer and right column (c,f) with yttria interlayer. The coloring reflects the crystallographic direction along the wire axis, corresponding to the inset in (c). Boundaries are highlighted in (d-f): High angle boundaries with disorientation angles above 15° in black and low angle boundaries with disorientation angles between 2° and 15° in light brown. In the boundary maps (d-f) the colors representing orientations are rendered transparent.

4. Discussion

For an understanding of the annealing phenomena in the single tungsten fiber-reinforced tungsten composites it is essential to consider that the two different tungsten constituents are produced in a total different manner: tungsten wires are produced by large plastic deformation through wire drawing where an abundance of lattice defects becomes stored in the deformation structures. The chemically vapor deposited tungsten matrix, on the other hand, is deposited atom-by-atom so that almost perfect crystalline lattices are built containing only a small number of growth defects, mainly boundaries between differently oriented grains. In this manner, the stored energy density

being the driving force for thermally activated restoration phenomena occurring during annealing is entirely different for both constituents. This essential difference forms the basis for an interpretation of the different processes occurring in these W_f/W composite during annealing.

4.1 Microstructure evolution in the wire

During plastic deformation by wire drawing, dislocations are formed in the drawn tungsten wires. They get stored in the deformation structure and form dislocation boundaries. Grains become elongated and aligned along the drawing direction; the resulting microstructure consists of fibrous grains showing a strong fiber texture. At elevated temperatures, this deformation structure will undergo restoration processes, in particular, recovery and recrystallization, to lower the energy stored in the defect content, mainly in form of dislocations and dislocation boundaries. As chemical vapor deposition of the tungsten matrix is performed at relatively low temperatures below 620 °C [30] (compared to the expected operation temperatures in fusion reactors and the annealing temperature of 1400 °C used in this study) occurrence of only slight recovery is expected during CVD and no recrystallization is observed. The microstructure of the wire in the as-processed condition resembles the expectations from the drawing process with very small grains (with a resolved boundary spacing of 0.42 µm) and a strong alignment of the <110> direction with the wire axis.

Significant changes are observed after isothermal annealing at 1400 °C: a zone of larger grains with average boundary spacing up to 1 µm develops in a certain distance from the wire center up to the wire edge. At the same time, the strong alignment of the <110> directions gets weaker. The resolved grains of slightly larger size might be the result of either primary recrystallization of the deformation structure by moving high angle boundaries or a process commonly referred to as *recrystallization in-situ* which is essentially extended recovery by subgrain growth [13]. Due to the strong texture with alignment of <110> directions along the wire axis in the

deformation structure, deformed grains are quite often separated by low angle boundaries only, rendering a distinction between subgrains and grains somehow inapplicable. Nevertheless, occurrence of primary recrystallization by nucleation of new defect-free grains and migration of HABs (instead of *recrystallization in-situ*) seems more likely to be the occurring phenomenon due to the development of larger grains with new orientations in the wire. (The new defect-free grains with crystallographic directions along the wire axis deviating from <110> and without any internal disorientations were neatly revealed from the orientation maps.) Comparing the different microstructures after different times of annealing, it becomes obvious that the extension of the large grain zone in the wire is progressing towards the wire center. Contrarily, one gets the impression that recrystallized grains in the wire do neither prefer growing radially, nor grow much further at all during continued annealing after their initial formation. The latter observation is supported by the quantitative analysis in Fig. 6. For radii between 40 µm and the position of the interlayer, i.e. within the zone of large grains in the wire, the spacing between high angle boundaries varies only slightly between 0.75 µm and 1 µm.

This restricted growth of the recrystallized grains and absence of further grain coarsening might be a consequence of either orientation pinning within the wire or Zener pinning by potassium bubbles due to the doping of the wire: Due to the sharp texture of the drawn wire with <110> directions strongly aligned to the wire axis, a moving high angle boundary of a recrystallization nucleus may encounter a deformed grain with similar orientation, turn into low angle boundary and get pinned due its lower mobility [38]. Alternatively, the potassium bubbles purposely created during the manufacturing process by insoluble potassium restrict the motion of boundaries by Zener pining (cf. [26]) and hinder the further growth of recrystallized grains. Under the present annealing conditions, the recrystallized grains in the wire of the single fiber composites with an erbia interlayer may not have reached the critical grain size for overcoming boundary pinning by potassium bubbles [39]. Further quantitative analysis of the microstructural evolution along the outlined lines is required to clarify the details and planned for the future.

4.2 Microstructure evolution in the matrix

The microstructure of the chemically vapor deposited tungsten matrix does not contain any deformation-induced defects (as dislocation and dislocation boundaries which would cause orientation variations within the individual grains). Moreover, the as-deposited matrix consists of a grain structure with wedge-shaped grains along the radial deposition direction. In the vicinity of the erbia interlayer, the HAB spacing is small, almost comparable to the one in the wire. (The latter comparison must to be considered with caution as the chosen step size of the orientation maps may affect the quantitative result.) In the absence of a deformation structure neither recovery, nor recrystallization can occur. In case of recrystallization, not only the driving force is lacking, recrystallization nuclei cannot be formed from other lattice defects either. The only possible restoration process is grain growth driven by reduction of the energy stored in the grain boundaries themselves, i.e. grain coarsening [13,14].

After annealing at 1400 °C, the occurrence of rather large grains in the immediate vicinity of the oxide interlayer is observed. In the region between 75 µm and 85 µm, the boundary spacing increased from about 0.5 µm to 4 µm during 28 h of annealing. This exceptional increase in boundary spacing by a factor 8 outperforms clearly the observed increase in regions further out, e.g. at around a radius of 100 µm the boundary spacing increased from 1.8 µm to 2.8 µm, i.e. by a factor 1.5 only.

Further out in the matrix beyond the large grain zone, no major changes in the microstructure due to annealing at 1400 °C are seen. For instance, the HAB spacing and its dependence on the radius as described by the slope φ remains almost unaltered. This is in accordance with several investigations on the lateral growth of columnar grains in CVD tungsten where very little growth was reported for annealing at 1520 °C for 100 h [40] or at 1500 °C for 3 h [41].

The major difference in grain growth in the vicinity of the interlayer and regions further out in the matrix is caused by the peculiar microstructure after deposition. In the outer regions of the

CVD matrix, the boundary density and hence the driving force for grain growth is rather low. Additionally, the wedge shaped grains separated by relatively long and straight boundary segments render curvature-driven grain growth by motion of triple junctions rather slow (due to the absence of both, curved boundaries and triple junctions), if not impossible.

On the other hand, the higher boundary densities closer to the interlayer exert a higher driving force for restoration due to the higher stored energy density. Grains in the vicinity of the interlayer are not extremely elongated as those further out and possess a growth advantage due to their morphology. Initially, some grains in that region start to grow at the expense of their neighbors and gain a slight size advantage. Due to the microstructure consisting of wedge-shaped grains even a slightly larger azimuthal size of some grains will turn into a growth advantage: the mobile growth front along a perimeter will border more radially aligned boundaries (of wedge-shaped grains) on the outside than on the inside. The growth front will continue to move outwards due to the slightly larger azimuthal grain size and slightly lower boundary density behind. In this manner, some grains can get a decisive growth advantage and will be able to undergo exceptional growth. The process does not proceed in a homogeneous manner and should not be considered as homogeneous grain coarsening or normal grain growth. Due to the growth advantage of a few grains in the microstructure, the process must rather be envisaged as abnormal grain growth (also termed secondary recrystallization) [42] with a few exceptionally growing grains. If wedge-shaped grains on the outside of the growth front are replaced by abnormally growing wedge-shaped grains an existing growth advantage will prevail during growth and abnormally growing grains are expected to continue to grow radially without limitation.

4.3 Microstructure evolution at the interlayer

Extrusion and intrusions were observed from secondary electron images and the orientation maps for oxide interlayers as well as the interface between wire and matrix in the absence on an

interlayer. These deviations of the wire from a cylindrical shape are inherited from the manufacturing process. During wire drawing, geometrical imperfections of the die (or alien material deposited at the surface) result in drawing grooves on the wire surface. This commonly undesired drawing scars may actually have positive effects on the mechanical behavior of tungsten-fiber reinforced tungsten composites as grooves increase the surface area between wire and matrix and hence the energy required for relative motion between wire and matrix, if the cohesion between both is not impeded otherwise.

The presence of an interlayer plays a decisive role for the development of the two zones of large grains during annealing: For the composites with an interlayer, the wire region can be clearly distinguished from the matrix region by the presence of the non-indexed interlayer in Figs. 7(b-c). The two large grain zones are clearly separated by the erbia or yttria interlayers and in general no growth of grains from the large grain zone in the matrix into the wire is observed. Only at certain locations where the erbia or yttria interlayer seems disrupted, larger grains from the matrix have seemingly invaded the wire region. In some occasions where in-growth is observed and the interlayer seems to be still in place, it is believed that in-growth occurred through holes in the interface at a different depth in the specimen. Such imperfections in the rare-earth oxide interlayers might originate from the magnetron sputtering process occurring in two steps to coat the entire wire (such imperfections are revealed by tungsten bridges from wire to matrix through yttria interlayers [43]) or formed during annealing by disintegration of the interlayer (the latter being frequently observed for yttria interlayers and much less for erbia interlayers [43]).

The single fiber composite without an interlayer shows an entirely different behavior (cf. Figs. 7a): After annealing the original interface between matrix and wire cannot be located any longer. Two zones with large grains have developed in the wire and matrix, respectively, but extraordinarily large grains have invaded the wire. Grains growing abnormally in the tungsten matrix must have achieved such an enormous size advantage (above a critical size for effective Zener pining), that they are able to grow into outer parts of the wire at the expense of the

recrystallized grains (in the large grain zone there) despite the inhibition of the boundary motion by the potassium bubbles. It becomes obvious from Fig. 7a, that these abnormally growing grains become much larger than the ones in the composites with an interlayer in Figs. 7(b-c). With further annealing time, it can expected that the abnormally growing grains will invade the tungsten wire entirely. As a consequence, the benefit of the tungsten wires on the improved mechanical properties of the fiber-reinforced composite will be lost, not only due to the removal of the deformation structure in the wire, but also due to the complete removal of any interface between wire and matrix. While embrittlement of the wire by recrystallization may not impede the pseudo-ductility significantly [30], the loss of any debonding capability due to the loss of an interface will be detrimental. A protective interlayer between wire and matrix is therefore of uttermost importance for preserving the tungsten wires in the composite – even if they undergo recrystallization.

5. Conclusions and Outlook

As a model system for more complex tungsten fiber-reinforced tungsten composites, single fiber composites containing a single drawn potassium-doped tungsten wire in a chemically vapor deposited tungsten matrix are investigated. The thermal stability of three different systems with or without an erbia or yttria interlayer is characterized. During annealing at 1400 °C for up to 28 d, two rather different zones develop both showing much larger grains than in the as-processed condition. As indicated by subtle, but notable orientation changes, new defect-free grains (without any deformation structure or internal orientation variations) form in the wire by primary recrystallization through nucleation of defect-free grains and boundary migration. These emerging grains are larger than in the drawn state, but their growth seems limited to a certain size by either orientation pinning or pinning at potassium bubbles. Suppression of further growth of the recrystallized grains by Zener pinning would indicate that potassium bubbles which might have grown to larger sizes [44] are still persisting in the wire. In the CVD matrix, grains in the vicinity of the interlayer with moderate aspect ratios grow abnormally at the expense of others leading to a

corona of (almost) equiaxed grains. The wedge-shaped grains in the further distant parts of the matrix are only slightly affected by the heat treatment.

The rare earth oxide interlayers provide an effective barrier for separating the restoration process occurring in both parts: primary recrystallization in the wire and abnormal grain growth (or secondary recrystallization) in the matrix. The motion of grain boundaries is blocked by the alien phase as long as the interlayer remains intact and no pathways between the two different parts exist. Without the presence of such an interlayer, the restoration processes in both regions occur coupled and grains of the matrix having achieved a major size advantage there start to grow into the recrystallized outer regions of the wire without an oxide phase preventing their growth and seemingly without effective boundary pinning by potassium bubbles due to their size. In this manner, the presence of an oxide interlayer between the wire and the CVD matrix is indispensable for the thermal stability of W_f/W composites. The potassium-doped wire can only retain its superior thermal stability if shielded from the CVD matrix by an interlayer and no intergrowth occurs.

Acknowledgements

This work has been carried out partially within the framework of the EUROfusion Consortium and has received funding from the Euratom research and training programme 2014-2018 and 2019-2020 under grant agreement No 633053. The views and opinions expressed herein do not necessarily reflect those of the European Commission.

Data Availability

The raw/processed data required to reproduce these findings cannot be shared at this time as the data also forms part of an ongoing study.

[1] F. Romanelli, EFDA, Fusion Electricity: A roadmap to the realisation of fusion energy, (2012) 1–75. https://doi.org/ISBN 978-3-00-040720-8.

[2] J.H. You, E. Visca, C. Bachmann, T. Barrett, F. Crescenzi, M. Fursdon, H. Greuner, D. Guilhem, P. Languille, M. Li, S. McIntosh, A. V. Müller, J. Reiser, M. Richou, M. Rieth, European DEMO divertor target: Operational requirements and material-design interface, Nucl. Mater. Energy. 9 (2016) 171–176. https://doi.org/10.1016/j.nme.2016.02.005.

[3] J.W. Davis, V.R. Barabash, A. Makhankov, L. Plöchl, K.T. Slattery, Assessment of tungsten for use in the ITER plasma facing components, J. Nucl. Mater. 258–263 (1998) 308–312. https://doi.org/10.1016/S0022-3115(98)00285-2.

[4] E. Lassner, W.-D. Schubert, Tungsten: Properties, Chemistry, Technology of the Element, Alloys, and Chemical Compounds, 1st Ed., Springer, Boston, MA, 1999. https://doi.org/10.1007/978-1-4615-4907-9.

[5] R.G. Abernethy, Predicting the performance of tungsten in a fusion environment: a literature review, Mater. Sci. Technol. 0836 (2016) 1–12. https://doi.org/10.1080/02670836.2016.1185260.

[6] E.E. Bloom, R.W. Conn, J.W. Davis, R.E. Gold, R. Little, K.R. Schultz, D.L. Smith, F.W. Wiffen, Low activation materials for fusion applications, J. Nucl. Mater. 122 (1984) 17–26. https://doi.org/10.1016/0022-3115(84)90570-1.

[7] B. Gludovatz, S. Wurster, A. Hoffmann, R. Pippan, Fracture toughness of polycrystalline tungsten alloys, Int. J. Refract. Met. Hard Mater. 28 (2010) 674–678. https://doi.org/10.1016/j.ijrmhm.2010.04.007.

[8] D. Rupp, R. Mönig, P. Gruber, S.M. Weygand, Fracture toughness and microstructural characterization of polycrystalline rolled tungsten, Int. J. Refract. Met. Hard Mater. 28 (2010) 669–673. https://doi.org/10.1016/j.ijrmhm.2010.05.006.

[9] D. Rupp, S.M. Weygand, Experimental investigation of the fracture toughness of polycrystalline tungsten in the brittle and semi-brittle regime, J. Nucl. Mater. 386–388 (2009)

591–593. https://doi.org/10.1016/j.jnucmat.2008.12.184.

[10] B. Gludovatz, S. Wurster, T. Weingartner, A. Hoffmann, R. Pippan, Influence of impurities on the fracture behaviour of tungsten, Philos. Mag. 91 (2011) 3006–3020. https://doi.org/10.1080/14786435.2011.558861.

[11] P. Schade, 100 years of doped tungsten wire, in: Int. J. Refract. Met. Hard Mater., 2010: pp. 648–660. https://doi.org/10.1016/j.ijrmhm.2010.05.003.

[12] C. Bonnekoh, A. Hoffmann, J. Reiser, The brittle-to-ductile transition in cold rolled tungsten: On the decrease of the brittle-to-ductile transition by 600 K to − 65 °C, Int. J. Refract. Met. Hard Mater. 71 (2018) 181–189. https://doi.org/10.1016/j.ijrmhm.2017.11.017.

[13] F. Haessner, Systematic survey and basic problems of recrystallization, in: Recryst. Met. Mater., Riederer Verlag GmbH, 1978: pp. 1–10.

[14] F.J. Humphreys, M. Hatherly, Recrystallization and Related Annealing Phenomena, Elsevier B.V., 2004. https://doi.org/10.1016/b978-0-08-044164-1.x5000-2.

[15] A. Alfonso, D. Juul Jensen, G.N. Luo, W. Pantleon, Recrystallization kinetics of warm-rolled tungsten in the temperature range 1150-1350 °C, J. Nucl. Mater. 455 (2014) 591–594. https://doi.org/10.1016/j.jnucmat.2014.08.037.

[16] A. Alfonso, D. Juul Jensen, G.N. Luo, W. Pantleon, Thermal stability of a highly-deformed warm-rolled tungsten plate in the temperature range 1100-1250 °C, Fusion Eng. Des. 98–99 (2015) 1924–1928. https://doi.org/10.1016/j.fusengdes.2015.05.043.

[17] Ciucani U, Pantleon W, Stagnant recrystallization in warm-rolled tungsten in the temperature range from 1150 °C to 1300 °C, Fusion Eng. Des. (2019). https://doi.org/10.1016/j.fusengdes.2019.01.088.

[18] U.M. Ciucani, A. Thum, C. Devos, W. Pantleon, Isothermal annealing of thin rolled tungsten plates in the temperature range from 1300 °C to 1400 °C, Nucl. Mater. Energy. 15 (2018). https://doi.org/10.1016/j.nme.2018.03.009.

[19] U.M. Ciucani, A. Thum, C. Devos, W. Pantleon, Recovery and recrystallization kinetics of

differently rolled, thin tungsten plates in the temperature range from 1325 °C to 1400 °C, Nucl. Mater. Energy. 20 (2019) 100701. https://doi.org/10.1016/j.nme.2019.100701.

[20] C. Bonnekoh, U. Jäntsch, J. Hoffmann, H. Leiste, A. Hartmaier, D. Weygand, A. Hoffmann, J. Reiser, The brittle-to-ductile transition in cold rolled tungsten plates: Impact of crystallographic texture, grain size and dislocation density on the transition temperature, Int. J. Refract. Met. Hard Mater. 78 (2019) 146–163. https://doi.org/10.1016/j.ijrmhm.2018.09.010.

[21] P. Lied, C. Bonnekoh, W. Pantleon, M. Stricker, A. Hoffmann, J. Reiser, Comparison of K-doped and pure cold-rolled tungsten sheets: As-rolled condition and recrystallization behaviour after isochronal annealing at different temperatures, Int. J. Refract. Met. Hard Mater. 85 (2019). https://doi.org/10.1016/j.ijrmhm.2019.105047.

[22] Y. Mutoh, K. Ichikawa, K. Nagata, M. Takeuchi, Effect of rhenium addition on fracture toughness of tungsten at elevated temperatures, J. Mater. Sci. 30 (1995) 770–775. https://doi.org/10.1007/BF00356341.

[23] S. Wurster, B. Gludovatz, A. Hoffmann, R. Pippan, Fracture behaviour of tungsten-vanadium and tungsten-tantalum alloys and composites, J. Nucl. Mater. 413 (2011) 166–176. https://doi.org/10.1016/j.jnucmat.2011.04.025.

[24] M. Battabyal, R. Schäublin, P. Spätig, N. Baluc, W-2wt.%Y 2O 3 composite: Microstructure and mechanical properties, Mater. Sci. Eng. A. 538 (2012) 53–57. https://doi.org/10.1016/j.msea.2012.01.011.

[25] M. V. Aguirre, A. Martín, J.Y. Pastor, J. Llorca, M.A. Monge, R. Pareja, Mechanical properties of Y2O3-doped W-Ti alloys, J. Nucl. Mater. 404 (2010) 203–209. https://doi.org/10.1016/j.jnucmat.2010.07.016.

[26] C.S. Smith, Grains, phases, and interfaces - An interpretation of microstructure, Trans. Am. Inst. Min. Metall. Eng. 175 (1948) 15–51.

[27] J. Du, T. Höschen, M. Rasinski, S. Wurster, W. Grosinger, J.H. You, Feasibility study of a

tungsten wire-reinforced tungsten matrix composite with ZrOx interfacial coatings, Compos. Sci. Technol. 70 (2010) 1482–1489. https://doi.org/10.1016/j.compscitech.2010.04.028.

[28] J. Riesch, T. Höschen, C. Linsmeier, S. Wurster, J.H. You, Enhanced toughness and stable crack propagation in a novel tungsten fibre-reinforced tungsten composite produced by chemical vapour infiltration, Phys. Scr. 2014 (2014) 014031. https://doi.org/10.1088/0031-8949/2014/T159/014031.

[29] H. Gietl, J. Riesch, J.W. Coenen, T. Höschen, C. Linsmeier, R. Neu, Tensile deformation behavior of tungsten fibre-reinforced tungsten composite specimens in as-fabricated state, Fusion Eng. Des. 124 (2017) 396–400. https://doi.org/10.1016/j.fusengdes.2017.02.054.

[30] J. Riesch, J.Y. Buffiere, T. Höschen, M. Scheel, C. Linsmeier, J.-H. You, Crack bridging in as-fabricated and embrittled tungsten single fibre-reinforced tungsten composites shown by a novel in-situ high energy synchrotron tomography bending test, Nucl. Mater. Energy. 15 (2018) 1–12. https://doi.org/10.1016/j.nme.2018.03.007.

[31] R. Neu, J. Riesch, J.W. Coenen, J. Brinkmann, A. Calvo, S. Elgeti, C. García-Rosales, H. Greuner, T. Hoeschen, G. Holzner, F. Klein, F. Koch, C. Linsmeier, A. Litnovsky, T. Wegener, S. Wurster, J.H. You, Advanced tungsten materials for plasma-facing components of DEMO and fusion power plants, Fusion Eng. Des. 109–111 (2016) 1046–1052. https://doi.org/10.1016/j.fusengdes.2016.01.027.

[32] R. Neu, J.W. Coenen, C. Linsmeier, T. Höschen, M. Li, R. Neu, Chemically deposited tungsten fibre-reinforced tungsten – The way to a mock-up for divertor applications, Nucl. Mater. Energy. 9 (2016) 75–83. https://doi.org/10.1016/j.nme.2016.03.005.

[33] J. Du, J.H. You, T. Höschen, Thermal stability of the engineered interfaces in W/f/W composites, J. Mater. Sci. 47 (2012) 4706–4715. https://doi.org/10.1007/s10853-012-6339-9.

[34] F. Bachmann, R. Hielscher, H. Schaeben, Texture analysis with MTEX- Free and open source software toolbox, in: Solid State Phenom., Trans Tech Publications Ltd, 2010: pp. 63–68. https://doi.org/10.4028/www.scientific.net/SSP.160.63.

[35] P. Zhao, J. Riesch, T. Höschen, J. Almanstötter, M. Balden, J.W. Coenen, R. Himml, W. Pantleon, U. von Toussaint, R. Neu, Microstructure, mechanical behaviour and fracture of pure tungsten wire after different heat treatments, Int. J. Refract. Met. Hard Mater. 68 (2017) 29–40. https://doi.org/10.1016/j.ijrmhm.2017.06.001.

[36] E.S. Meieran, D.A. Thomas, Structure of drawn and annealed tungsten wire, Trans. Metall. Soc. Aime. 233 (1965) 937.

[37] A. Barna, I. Gaal, O. Geszti-Harkner, G. Radnoczi, L. Uray, The fibre structure of K-Si-Al doped tungsten wires, High Temp. - High Press. 10 (1978) 197–205.

[38] D. Juul Jensen, Effects of orientation on growth during recrystallization, in: Microstruct. Crystallogr. Asp. Recryst. (16th Risø Int. Symp., 1995: pp. 119–137.

[39] F.J. Humphreys, A unified theory of recovery, recrystallization and grain growth, based on the stability and growth of cellular microstructures. 2. The effect of second-phase particles, Acta Mater. 45 (1997) 5031–5039.

[40] Y.T. Auck, J.G. Byrne, Grain growth of chemical vapour deposited tungsten-22 wt % rhenium alloy, J. Mater. Sci. (1973) 559–564.

[41] Y. Lian, F. Feng, J. Wang, X. Liu, J. Song, Y. Wang, Z. Chen, J. Chen, No Effect of high temperature annealing on the microstructure and thermal shock resistance of tungsten coatings grown by chemical vapor deposition, J. Nucl. Mater. 513 (2019) 241–250. https://doi.org/10.1016/ j.jnucmat.2018.11.006.

[42] K. Detert, Secondary recrystallization, in: Recryst. Met. Mater., 2nd ed., Riederer Verlag GmbH, 1978: pp. 97–109.

[43] H. Gietl, Weiterentwicklung von wolframfaserverstärktem Wolframverbundwerkstoff für den Einsatz in der Fusion, Technical Univeristy of Munich, 2018.

[44] P. Schade, Potassium bubble growth in doped tungsten, Int. J. Refract. Met. Hard Mater. 16 (1998) 77–87.